Available online at www.sciencedirect.com
SCIENCE DIRECT
Acta Materialia 54 (2006) 2343–2351
Acta MATERIALIA
www.actamat-journals.com

A new approach to the modeling of SHS reactions: Combustion synthesis of transition metal aluminides

Silvia Gennari [a,*], Umberto Anselmi Tamburini [a,b], Filippo Maglia [a], Giorgio Spinolo [a], Zuhair A. Munir [b]

[a] INSTM, IENI, CNR, and Department of Physical Chemistry, University of Pavia, Viale Taramelli, 16, 27100 Pavia, Italy
[b] Department of Chemical Engineering and Materials Science, University of California, Davis, CA 95616, USA

Received 26 October 2005; received in revised form 9 January 2006; accepted 10 January 2006
Available online 10 March 2006

Abstract

A recently developed numerical simulation of self-propagating high-temperature synthesis (SHS) using an approach based on microscopic reaction mechanisms and utilizing appropriate physical parameters is applied to the SHS of a fairly large group of transition metal aluminides. The model was utilized to analyze temperature profiles and wave instability and the results were interpreted in terms of chemical and thermal effects. The effect of the particle size of the transition metal, the porosity of the reactant mixtures, and the dilution was investigated. The results are in good agreement with available experimental data.

Keywords: Self-propagating high-temperature synthesis; Transition metal aluminides; Modeling

1. Introduction

Combustion synthesis or self-propagating high-temperature synthesis (SHS) has received considerable attention in the last two decades as an alternative method for the synthesis of high-temperature materials. Beside its technological relevance, SHS is also of significant scientific interest, being the only example of an extremely fast chemical reaction completely confined in the condensed state. Despite the large number of investigations, knowledge of the microscopic reaction mechanisms involved in these processes is still quite limited. The combination of high reaction temperatures and high propagation rates makes it difficult to investigate experimentally such reactions using conventional techniques applied in solid-state reactivity studies. The lack of knowledge of the reaction mechanism makes difficult to anticipate the behavior of the reactions under conditions different from those employed experimentally.

Attempts to model SHS reactions to provide a better understanding of the operative mechanism have been made since the early 1970s. These approaches focused primarily on the macroscopic features of the propagation process. A simplified reaction mechanism based on the assumption of a single reaction step, derived from homogenous gas-phase combustion, was generally used in these earlier investigations [1]. Only recently more complex and realistic reaction mechanisms have been proposed. However, even in these cases the parameters controlling the microscopic reaction mechanism are usually optimized in order to obtain a good "fit" to the experimental results, with little attention to their intrinsic physical meaning [2,3]. A more useful approach would be to utilize parameters with a sound physical basis in order to validate the proposed microscopic reaction mechanism. When accomplished, such models make possible the prediction of the reaction behavior in situations that cannot easily be investigated experimentally.

Such an approach has been developed in general terms by the authors in previous publications [4–8]. In this work, we apply this approach to a large group of reactions, namely the formation of transition metal aluminides, to

* Corresponding author. Tel.: +39 0382987208; fax: +39 0382987575.
E-mail address: silvia.gennari@unipv.it (S. Gennari).

1359-6454/$30.00
doi:10.1016/j.actamat.2006.01.009

perform a systematic comparison with the available experimental data. The group of transition metal aluminides considered in this work (Ni–Al, Co–Al, Ti–Al, Nb–Al), share the same SHS reaction mechanism but are characterized by different thermodynamics and kinetics properties and hence show very different propagation modes.

The aim of the paper is twofold: to demonstrate the validity of the microscopic heterogeneous mechanism underlying the model and to show that a detailed microscopic mechanism involving a large number of simple interconnected elementary processes can produce results very close to the experimental observations, using experimental parameters with physical meaning. In this regard, this work represents a unique approach. As stated above, while comparisons between modeling and experimental results are relatively common in the SHS literature, none of these involves a detailed reaction mechanism. Typically, previous studies have been focused on the macroscopic behavior of the reaction.

Only parameters experimentally accessible will be discussed in this paper. The influence of parameters typical of the microscopic reaction mechanism, such as the kinetics of dissolution of the transition metal in liquid aluminum or the thermodynamic parameters related to the shape of the phase diagram have already been discussed elsewhere [9,10].

However, it must be pointed out that experimental data available in the SHS literature have significant limitations. Although the synthesis of transition metal aluminides has been extensively investigated, most of the available literature is qualitative in nature, with only few cases where the influence of reaction parameters on the propagation characteristics was investigated systematically and quantitatively. The effect of stoichiometry of the reactant mixture and the degree of dilution has been by far the most investigated aspect of these reactions. The dependence of combustion on other parameters, for example particle size, is virtually absent in the majority of the systems investigated. This makes it difficult to perform a through comparison with the modeling results even for systems that have been studied extensively, such as the Ni–Al system.

2. Modeling the SHS of transition metal aluminides

The simulation of an SHS process is based on the solution of a parabolic system of partial differential equations:

$$\begin{cases} C\dfrac{\partial T}{\partial t} = \nabla(\chi\cdot\nabla T) + \dfrac{2\cdot\sigma\cdot\varepsilon\cdot(T^4 - T_a^4)}{R} + \sum_i \dot{q}^i_{\text{chem}} \qquad (1) \\ \dot{q}^i_{\text{chem}} = f(x,y,z,T,t), \qquad (2) \end{cases}$$

where C represents the heat capacity per unit volume, χ the thermal conductivity, σ the Stefan–Boltzmann constant, ε the emissivity (set to 0.9 in these simulations) and T_a the ambient temperature (typically 298 K). In the present work, the equation has been written for a cylindrical sample of radius R (typically $R = 1$ cm) and length L (typically $L = 2$ cm). Eq. (1) is the Fourier law for heat transport, while Eq. (2) is a kinetic equation that describes the assumed microscopic chemical mechanism and, hence, the rate of heat evolution. This second equation includes as many chemical steps as required, taking into explicit account the heterogeneous aspects of the process.

The above system is solved for temperature, and hence initial and boundary conditions are given for T also. Typically the initial conditions are expressed as

$$T(x, t=0) = T_a \quad \text{for } 0 \leqslant x \leqslant L \qquad (3)$$

with x the distance along the axis of the sample of length L. The boundary conditions are given as

$$\begin{cases} T(0,t) = f_1(t) \\ T(L,t) = f_2(t) \end{cases} \qquad (4)$$

with f_2 accounting for heat input and output due to conduction, chemical reaction and phase transformation, radiation to the surroundings, and f_1 being an ignition function that represents the energy pulse obtained from the igniter. This latter is normally given as

$$f_1(t) = T_a + (T_p - T_a)\exp\left[-\frac{(t-\mu)^2}{2\sigma^2}\right] \qquad (5)$$

with T_a being room temperature, T_p the maximum temperature reached by the igniter, σ the time range and μ the time lag of ignition.

As graphically summarized in Fig. 1, the method chosen basically uncouples the solution of heat transport (solved for the whole sample and hence referred to as macrokinetics) from the solution of the chemical steps, each being solved at the level of a single particle and referred to as microkinetics. The present simulation approach is specifically built to focus on the heterogeneous aspects of a SHS process, and is based on a microscopic reaction mechanism that has been proposed by several authors on the basis of investigations performed mostly using the quenched front technique [11–13]. Such a model for the SHS of transition metal aluminides includes: (a) melting of Al (before which no reaction occurs), (b) diffusion-controlled dissolution of solid transition metal into liquid Al (the irreversible step), (c) eventual melting of the phases involved (if the temperature is sufficiently high), (d) precipitation and (eventual) melting of the intermetallic compound and (e) deposition of the $Al + Me_xAl_{1-x}$ eutectic mixture. Steps (a), (c), (d) and (e) are simply considered in terms of energy balance, while the dissolution of the high-melting metal into the molten pool is governed by an explicit kinetic law [14]. It should be noted that the dissolution coefficients used in the present work have all been obtained from isothermal dissolution experiments performed by our group [15]. The values used are reported in Appendix A.

The Fourier equation describing the heat transfer on the macroscopic scale is solved using the finite difference Crank–Nicolson algorithm. At each time step of the

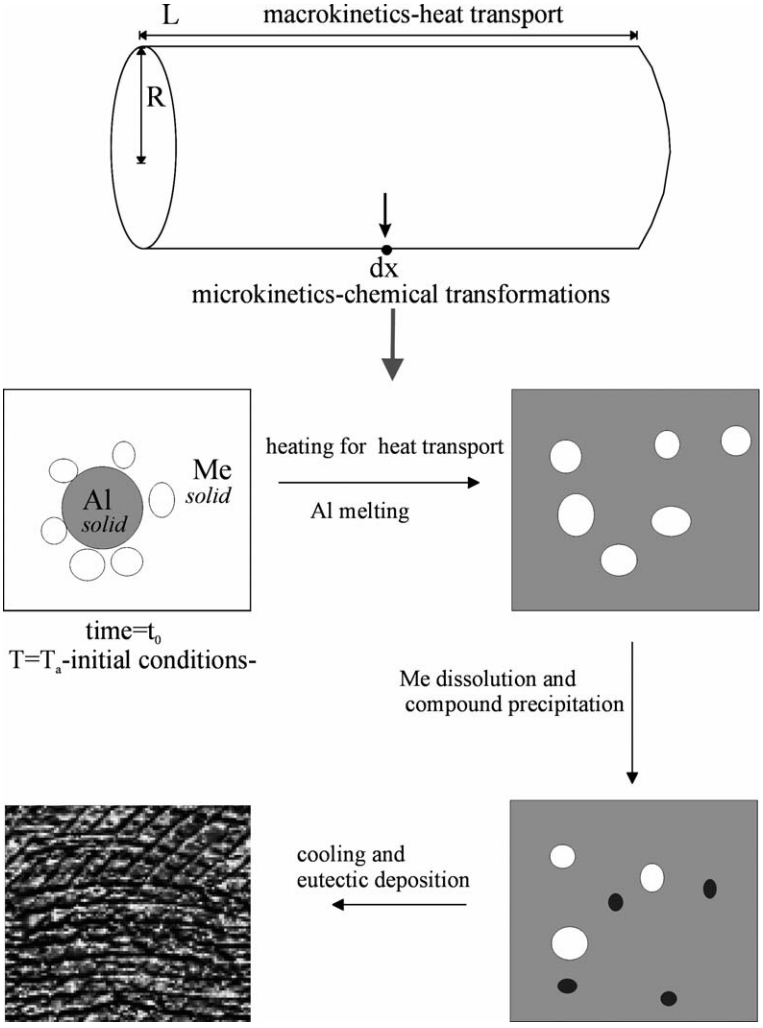

Fig. 1. Graphical scheme of the simulation process.

solution the amount of transition metal dissolved in the liquid (the irreversible steps) is calculated and the amount and composition of the relevant phases according to the phase diagram are calculated. The amount of heat associated with these processes is then passed back to the Fourier equation, which is then solved for temperature of the next time step. The thermodynamic description of the systems assumes great relevance in such a chemically oriented model and has been given using the widely accepted CALPHAD approach. Parameter values for each system have been obtained from the literature as reported in Appendix A. More information on the general concepts underlying our computational approach can be found in previous publications [4–10].

3. Results and discussion

3.1. Temperature profile

Experimentally, the temperature profile is generally obtained at one point on the sample, using a thermocouple or an optical pyrometer. As we will demonstrate, the shape of the temperature profile is strongly dependent on the details of the microscopic reaction mechanism. SHS processes for the formation of transition metal aluminides are characterized by a typical temperature profile, such as the one shown in Fig. 2 for the SHS of NiAl. It is characterized by a very sharp first peak, which is usually followed by a much broader second peak or by a plateau. Although this profile is quite common and has been reported in the literature, no quantitative explanation has been presented for the presence of the two maxima. Fig. 3(a) shows the calculated temperature profile as a function of time for the SHS of NiAl with $x_{Ni} = 0.49$, a particle radius r_0 of 50 μm and a thermal conductivity $\chi = \chi_{bulk}/10$. The temperature profile reproduces reasonably well the shape of the experimental curve of Fig. 2, showing an initial sharp peak followed by the much broader second peak. However, the timescale in this simulation is an order of magnitude lower than the experimental data of Fig. 2. This is due to the high value of thermal conductivity used for this simulation compared to the conductivity values typical of powder

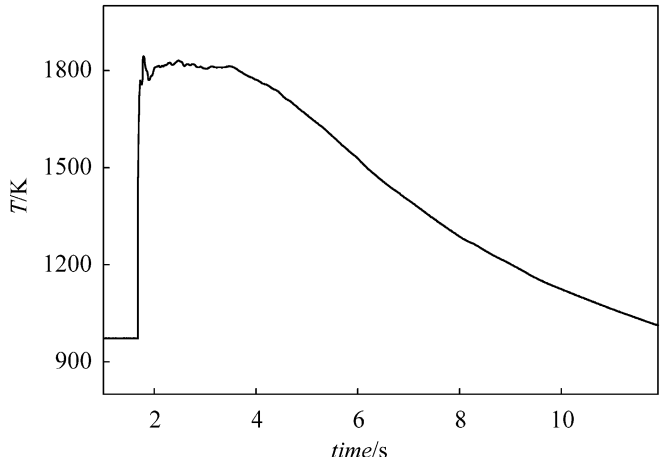

Fig. 2. Experimental profile of temperature for the SHS of NiAl. Ni grain size <10 μm.

compacts [16]. A detailed analysis of the propagation characteristics of the SHS as a function of thermal conductivity has been discussed in previous works [8,9,17].

Some aspects of the temperature profile can be related to the chemical changes accompanying the process. Fig. 3(b) depicts the phase evolution in the small region across the combustion front. These results are obtained using a simulation made with the same parameters as used in Fig. 3(a). In Fig. 3(b) the front propagates from right to left. When the temperature reaches the melting point of Al (point A in the figure) the solid transition metal (dotted line, left axis) begins to dissolve in the liquid leading to an increase in the amount of liquid phase (dashed line, left axis) until it reaches a maximum value, after which the solid intermetallic compound (dash-dot-dot line, left axis) begins to precipitate. The large amount of heat released by the precipitation of the compound is responsible for the first, sharp temperature spike in the temperature profile (point C in the figure). However, no further chemical reaction or phase transformation takes place outside this region, as shown on a larger scale in Fig. 3(c) where the amount of all phases is seen to remain constant after the first sharp reaction front. This implies that the second broad peak that is observed in Figs. 2 and 3(a) cannot be related to any heat release/absorption due to phase transformations and/or to a chemical process.

An alternative explanation, however, can be found in the complex mechanism that causes propagation instabilities in this family of reactions. As discussed in more details elsewhere [8,9,17], the SHS reaction of transition metal aluminides is frequently characterized by oscillatory propagation modes. The onset of these oscillations is controlled by a balance between system characteristics (ΔH_{react}, dissolution rate and thermal conductivity) and process variables (porosity and reactant grain size). The intrinsic system properties for the SHS process for the formation of transition metal aluminides are such that oscillations are observed for a large range of process parameters. Fig. 4

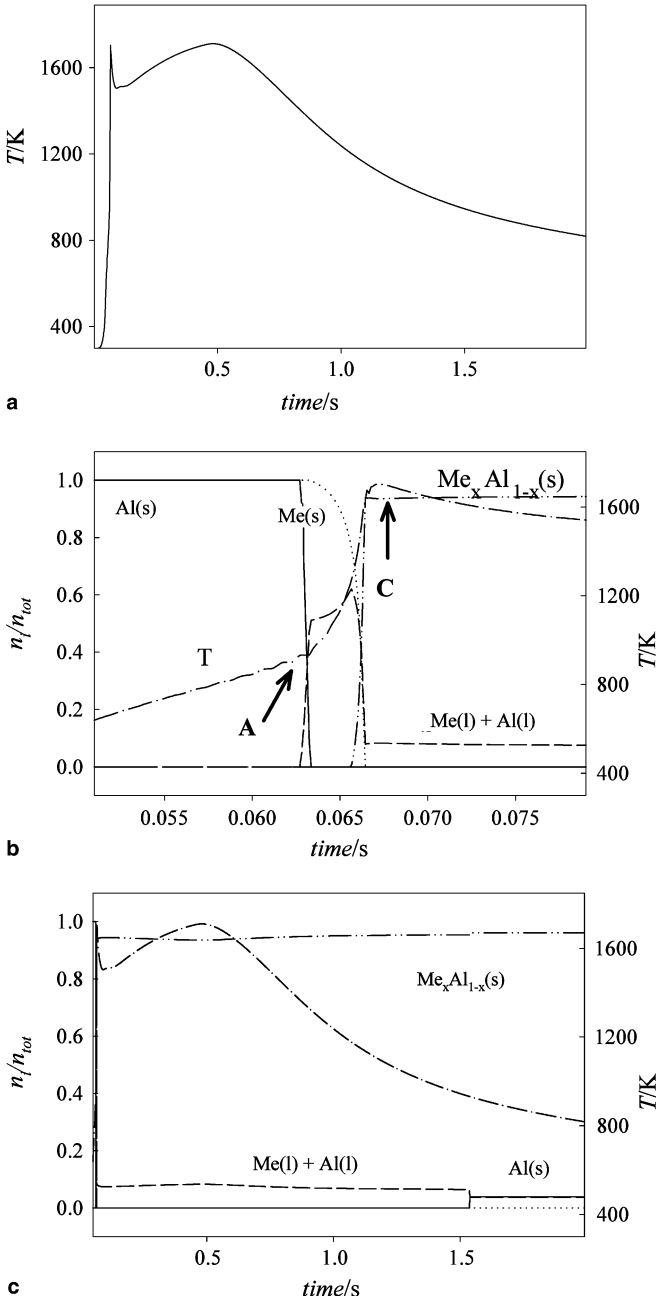

Fig. 3. Simulated temperature profile for the SHS of NiAl, with $x_{Ni} = 0.49$, $r_0 = 50$ μm and $\chi = \chi_{bulk}/10$, and enlargement of the temperature spike region for solid aluminum (continuous line, left axis), solid Ni (dotted line, left axis), solid compound (dash-dot-dot line, left axis), total amount of liquid (dashed line, left axis) and temperature (dash-dot line, right axis). n_i represents the moles per unit volume of a component in a certain phase. For simplicity reasons, n_i is normalized on the total number of moles available n_{tot} of the same component in the actual simulation run.

shows the combustion characteristics associated with a typical oscillating reaction in the formation of NiAl. As shown in the graph at the top of the figure when this situation occurs, the propagation rate of the combustion front changes considerably with time. These oscillations, however, are often characterized by a time and space scale that makes it difficult to observe them experimentally. Due to

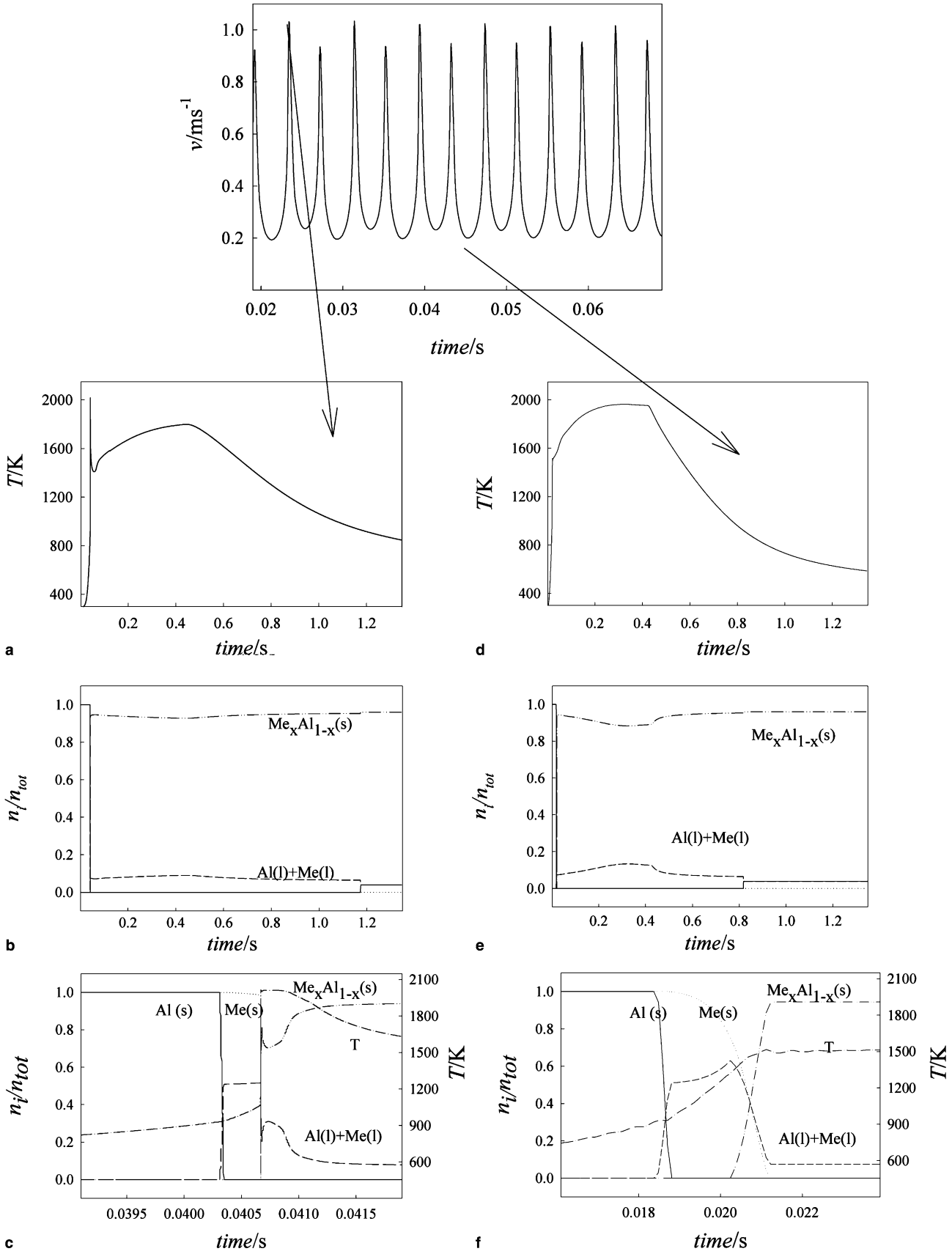

Fig. 4. Temperature and amounts of reactants and compound in the various phases as a function of time for space points corresponding to the maximum (a–c) and minimum (d–f) of propagation wave speed. In (b–f) the continuous line shows solid Al, the dots solid transition metal, the dashed-dotted line temperature (right axis), the dashed line total amount of liquid and the dash-dot-dot line solid compound.

the presence of the oscillations the temperature profile will be different at different locations of the sample. Fig. 4(a) and (d) show the temperature profiles corresponding to regions pertaining to the highest (Fig. 4(a)) and lowest (Fig. 4(d)) propagation rates. The two temperature profiles are quite different; Fig. 4(a) shows the presence of a sharp spike at the leading edge of the combustion front while Fig. 4(d) shows only a broad temperature peak. The phase evolution accompanying the movement of the combustion front in the two regions is shown in Fig. 4(b) and (e), respectively. Since the reaction is confined to a very small region, an expanded view of the combustion front is shown in Fig. 4(c) and (f), respectively. From Fig. 4(c) it can be inferred that the first temperature spike observed in Fig. 4(a) is associated with the precipitation of the intermetallic phase from the melt. Fig. 4(c) shows that the heat released by this process may be sufficient to raise the temperature above the melting point of the intermetallic compound itself, producing a quite complex phase evolution. In contrast, no sharp temperature spike is observed when the propagation wave velocity is at a minimum (Fig. 4(d)–(f)). In this case the process of dissolution and precipitation is spread over a fairly large region. It is also important to point out that there is no apparent connection between the broader temperature peak (following the leading edge) and any chemical reaction or phase transformation process. Thus the second peak can then only be explained as a thermal front. This suggests that the oscillating behavior is the results of a "decoupling" between the propagation of the thermal and chemical fronts. According to this model the "chemical" front (associated with the dissolution–precipitation process) tends to "run away", hence creating regions of localized high temperature that propagate much faster than the thermal wave. These spikes then fade away when they reach a region of the sample too cold to sustain the chemical process. As a result of that, the chemical front keeps moving back and forth with respect to the thermal front producing the oscillating behavior [9]. In these systems, however, this dynamic behavior is too fast to be detected by the techniques usually used in the determination of the temperature profiles.

3.2. Effect of particle size

The size of reactant particles has been recognized as an important parameters in defining the dynamic behavior of an SHS process, and hence the composition and microstructure of the resulting products [18–23]. Despite that, a systematic analysis of the dependence of wave velocity on the particle size of the reactants has not been investigated for most systems. An interesting exception is represented by the relative abundance of investigations demonstrating a lack of influence of the size of the Al particle on the macrokinetic behavior of the SHS process, indirectly demonstrating that Al is molten at the start of the reaction [11–13,24,25].

The influence of particle size r of the transition metal on the velocity of propagation v for various aluminides as calculated in this study is shown in Fig. 5, plotted as v vs. $1/r$. The figure also shows, for comparison, available experimental results reported in the literature. For the Ni–Al system, for which most experimental determinations are available, wave velocity values were reported by Maslov ($3 < v < 9$ cm s^{-1} [26]), Naiborodenko ($v = 4$ cm s^{-1} [24,25]) and Podergin ($v = 1.23$ cm s^{-1} [27]). In this figure the experimental values are compared with a curve obtained simulating the propagation for $0.1 < r_0$ (Ni) < 50 μm. Particle size values lower that 0.1 μm were not considered since experimentally such sizes are difficult to obtain, while the largest particle size for every system corresponds to the ignition limit under standard ignition conditions. In all the simulations reported in Fig. 5, an effective value of thermal conductivity close to the experimentally observed one for compact of powders ($\chi_{eff} = \chi_{bulk}/70$) was used for all systems.

Fig. 5 shows a fairly good agreement between the relatively few reported experimental data and the calculated values for all systems for which experimental data are available: (a) CoAl [28], (b) NiAl [24–27], (c) TiAl [29] and (d) $NbAl_3$ [30]. It is worth noting once again that the numerical values for the parameters corresponding to the individual physicochemical processes involved in the mechanism are experimental values taken from the literature and have not been modified in order to obtain a good fit with the experimental combustion rates. In all four SHS reactions, the wave velocity has an almost linear dependence with the inverse of particle size for large particle sizes ($r_0 > 1$ μm), the region in which experimental values are available. No experimental data have been reported for smaller particles sizes, where a plateau of the calculated curves is reached. The velocity at the onset of the plateau depends on the system examined, $v_{CoAl} = 5.3$ cm s^{-1}, $v_{NiAl} = 8.7$ cm s^{-1}, $v_{TiAl} = 3.3$ cm s^{-1}, $v_{NbAl3} = 3.0$ cm s^{-1}. The lack of dependence on particle size over the range of the plateau indicates that dissolution of the transition metal into the molten pool is no longer the rate-determining mechanism of the SHS reaction, but other processes, such as precipitation or dissolution of the formed compound, become rate controlling.

3.3. Effect of porosity and dilution

In SHS experiments, a change in the porosity of the reactants influences the effective thermal conductivity and the energy per unit volume produced by the reaction [9,16,31]. Thus in order to be able to perform a direct comparison with the experimental results, the effects of porosity on energy per unit volume and thermal conductivity must be taken into consideration. The dependence of thermal conductivity on porosity has been modeled using the approach of Cunningham and Peddicord [32]. The details of such a model can be found in Appendix A. Modeling of the effect of porosity and thermal conductivity has been made previously for field-activated combustion synthesis [33].

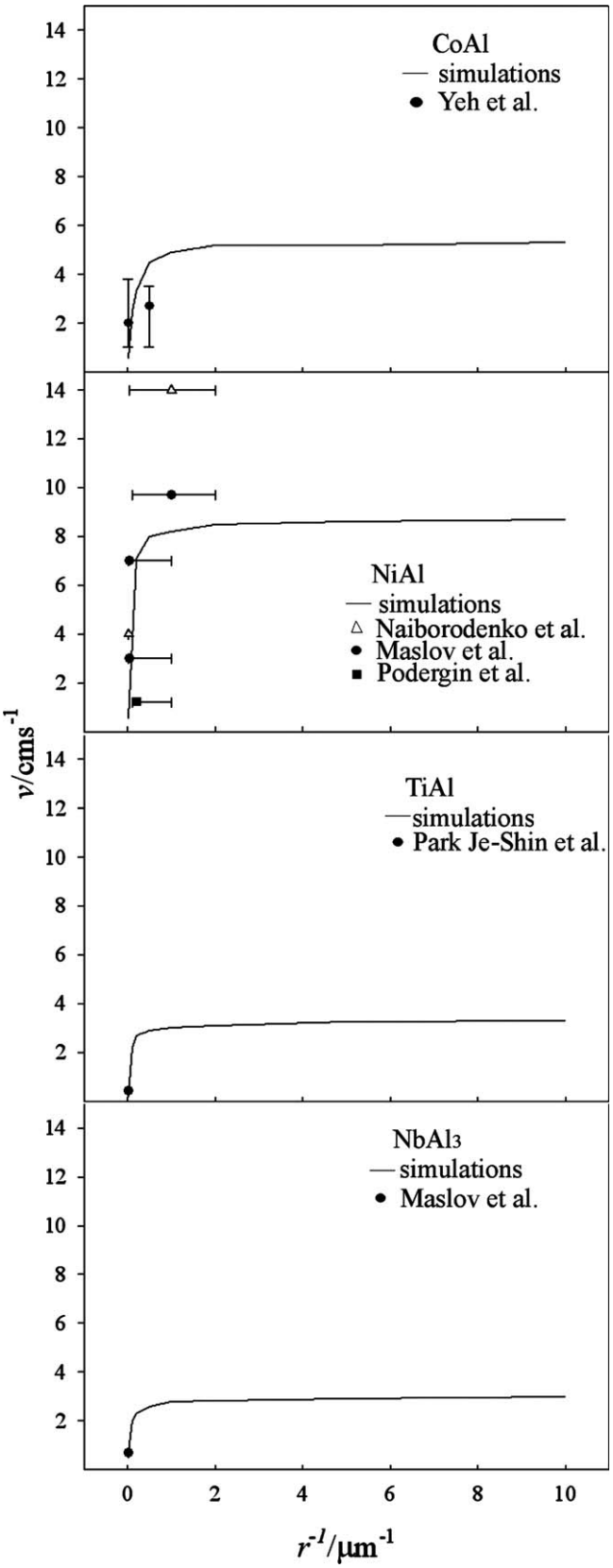

Fig. 5. Wave velocity as a function of the inverse of the high-melting metal starting grain size (with $\chi = \chi_{bulk}/70$) for the SHS of CoAl, NiAl, TiAl and $NbAl_3$. The continuous line refers to simulation results, the dots to experimental results for CoAl [28], NiAl [24–27], TiAl [29] and $NbAl_3$ [30].

A comparison of the simulated data for CoAl with experimental data reported by Yeh and Yeh [28] for a relatively small particle size (2 μm) is shown in Fig. 6. In order to reproduce the experimental conditions a temperature of pre-heating of 373 K was used. The trend of the increase of v with the relative density of the reactants is the same for the simulation and the experimental values.

Fig. 7 shows the calculated dependence of wave velocity on porosity (solid line) for the SHS of NiAl for the case of a relatively large particle size (50 μm). Experimental data for NiAl from Naiborodenko and Itin [24,25] are also plotted for comparison with the simulation results. The wave velocity increases as the porosity is decreased from 60% to 40%, reaching a maximum value (9 cm s^{-1} for

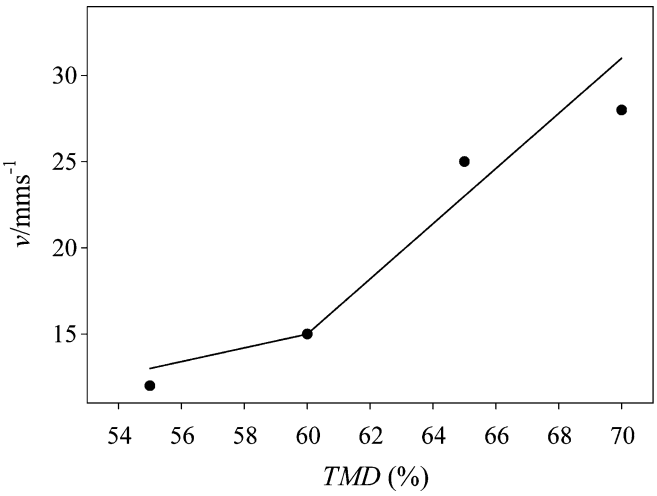

Fig. 6. Propagation speed for the SHS of CoAl as a function of per cent theoretical maximum density (TMD) of the starting mixture. Experimental data are from Yeh and Yeh [28]; the continuous line represents simulation results.

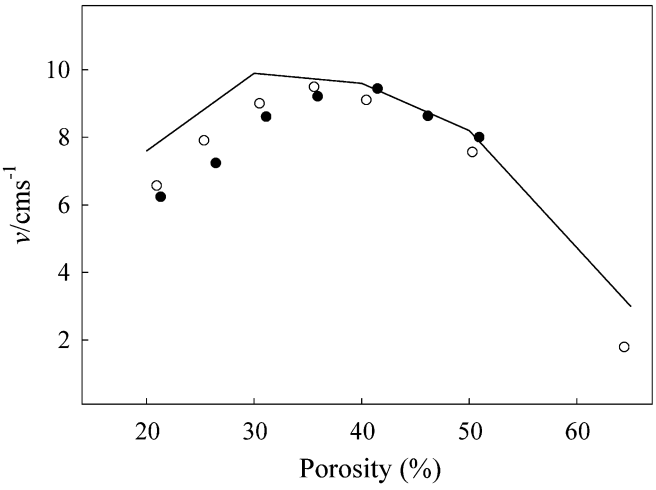

Fig. 7. Propagation speed for the SHS of NiAl as a function of porosity. The points indicate two sets of experimental data from Naiborodenko et al. [24,25] while the continuous line represents simulation results. Grain size used is $r_0 = 50$ μm.

porosity = 40% in experiments, and 9.9 cm s^{-1} for porosity = 30% in the simulation). When the porosity is further decreased, the velocity of propagation decreases. Such a behavior is largely expected and encountered in experiments, but has not been obtained previously using simulation methods that did not take into account the heterogeneous nature of the process. An increase in propagation wave velocity with a decrease in porosity reflects an increase of the energy per unit volume up to the maximum value. At that point, thermal conductivity and heat dissipation become dominant, leading to the decrease in propagation rate. With reference to Fig. 6, the occurrence of a maximum in the velocity depends on the materials characteristics and thus the absence of a maximum in this figure is the consequence of the limited range of density considered. It would be expected that at higher densities (>70%), a maximum would be observed, consistent with experimental observations, reported elsewhere [34].

The addition of a diluent is commonly practiced to decrease the exothermicity of an SHS reaction without influencing all the other parameters. In reality, however, the effect of such an addition to the starting mixture has three aspects: (a) it reduces the total amount of heat released by the process per unit volume, (b) adsorbs heat in proportion to the heat capacity of the diluent and (c) it alters the thermal conductivity of the system. Quantitative data on the effect of dilution in intermetallic systems are not found in the literature. Due to the low exothermicity of these systems, the addition of diluent is counterproductive. An exception comes from the work of Maslov et al., in which the effect of dilution on propagation velocity for the SHS of NiAl was investigated [26]. A comparison with our simulation performed taking into account all the effects caused by the addition of the diluent is shown in Fig. 8. The data refer to a starting Ni particle size of 10 μm, $\chi = \chi_{bulk}/70$ and $T_a = 298$ K (chosen to reproduce experimental conditions). The black circles in the figure are the experimental data of Maslov et al. [26], while the continuous line represents the simulation results. It can be seen that both the trend and the value of the velocity are in very good agreement for the simulation and the experiment.

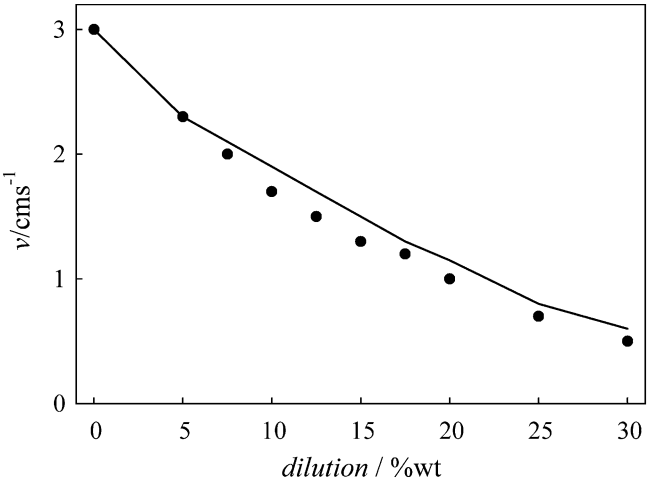

Fig. 8. Propagation speed as a function of dilution for the SHS of NiAl. Black dots refer to experimental data from Maslov et al. [30], while the continuous line shows results obtained from simulations. $r_{Ni} = 10$ μm, $\chi = \chi_{bulk}/70$ and room temperature of 298 K were used in simulations.

4. Concluding remarks

Using a model based on microscopic heterogeneous reactions, and on a solid–liquid interaction between liquid Al and solid transition metal, the SHS reactions of aluminides were simulated and compared to available experimental data. Based on appropriate physical parameters, the model provides results that are in good agreement with available experimental data. The model considered and interpreted the shape of the temperature profile associated with the reaction. The observed sharp and broad peaks are interpreted in terms of chemical and thermal effects. The observed instability of some reactions, giving rise to oscillatory wave propagation, was analyzed by the model and explained in terms of the chemical and heat transfer processes accompanying the reaction. The role of the particle size of the transition metal was modeled and the results were found to be in good agreement with experimental data. The effects of porosity (or relative density) of the reactant mixtures and the added diluents were considered, with the results shown to be in agreement with experimental observations.

Acknowledgement

This work was supported by a Grant from the National Science Foundation.

Appendix A

The relevant input parameters used in the present simulations are reported in this appendix.

- Thermodynamic data for the Ni–Al [35], Ti–Al [36], Co–Al [37] and Nb–Al [38] systems have been obtained from the literature using the SGTE standard and the CALPHAD (calculation of phase diagrams) approach. Details concerning this method and its application to the present simulation method can be found in previous papers [10,31] and in references therein.
- Dissolution coefficients Ω are given in an Arrhenius form. The pre-exponential term and activation energy have been obtained from experimental measurements in isothermal conditions performed by our group [15] and are as follows. Ni–Al: $\Omega_0 = 3 \times 10^{-7}$ m^2 s^{-1}, $E_a = 45.4$ kJ mol^{-1}; Co–Al: $\Omega_0 = 2.64 \times 10^{-6}$ m^2 s^{-1}, $E_a = 68.9$ kJ mol^{-1}; Ti–Al: $\Omega_0 = 4.1 \times 10^{-7}$ m^2 s^{-1}, $E_a = 19.9$ kJ ml^{-1}; Nb–Al: $\Omega_0 = 1.9 \times 10^{-9}$ m^2 s^{-1}, $E_a = 26.6$ kJ mol^{-1}.

- Thermal conductivity data for pure elements were obtained from the literature [39]. Thermal conductivity values for the mixture are given as a weighted combination of phases. Thermal conductivity values explored in the present simulations span the range $\chi_{bulk}/70 < \chi < \chi_{bulk}$. For a more reliable comparison with experiments, the effect of porosity p has also been modeled taking into account both its effect on energy per unit volume and on χ. The relationship between the two variables is given following the model of Cunninghan and Peddicord [32] for low porosity values, as $\chi = \chi_{bulk} f(p)$, with

$$\begin{cases} f(p) = e^{-2.14 \cdot p} & 0 \leqslant p < 0.30 \\ f(p) = 0.92 - 1.34 \cdot p & 0.30 \leqslant p < 0.50 \end{cases}$$

and the model of Koh et al. [40] for high porosity values, as

$$f(p) = \frac{1-p}{1+11p^2}.$$

- Starting high-melting metal grain size values used in the present work are $10^{-7} < r_0 < 5 \times 10^{-5}$ m.

References

[1] Merzhanov AG. Combust Flame 1969;13:143.
[2] Aldushin AP, Khaikin BI. Comb Expl Shock Waves 1974;10:273.
[3] Vrel D, Lihrmann JM, Tobaly P. J Mater Synth Proc 1994;2:179.
[4] Arimondi M, Anselmi-Tamburini U, Gobetti A, Munir ZA, Spinolo G. J Phys Chem B 1997;101:8059.
[5] Maglia F, Anselmi-Tamburini U, Gennari S, Spinolo G. Phys Chem Chem Phys 2001;3:489.
[6] Maglia F, Anselmi-Tamburini U, Gennari S, Spinolo G. J Phys Chem B 2002;106:6121.
[7] Gennari S, Maglia F, Anselmi-Tamburini U, Spinolo G. J Phys Chem B 2003;107:732.
[8] Gennari S, Maglia F, Anselmi-Tamburini U, Spinolo G. Intermetallics 2003;11:1355.
[9] Gennari S, Maglia F, Anselmi-Tamburini U, Spinolo G, Munir ZA. J Phys Chem B [submitted].
[10] Gennari S, Maglia F, Anselmi-Tamburini U, Spinolo G, Munir ZA. Comput Mater Sci [submitted].
[11] Fan Q, Chai H, Jin Z. Intermetallics 2001;9:609.
[12] Zhu P, Li JCM, Liu CT. Mater Sci Eng A 2002;329–331:57.
[13] Khina BB, Formanek B, Solpan I. Physica B 2005;355:14.
[14] Aaron HB, Fainstein D, Kotler GB. J Appl Phys 1970;41:4404.
[15] Milanese C. Ph.D. thesis, University of Pavia, Italy; 2001.
[16] Miura S, Terada Y, Suzuki T, Liu CT, Mishima Y. Intermetallics 2000;8:151.
[17] Gennari S, Maglia F, Anselmi-Tamburini U, Spinolo G. J Phys Chem B 2004;108:19550.
[18] Misiolek W, German RM. Mater Sci Eng A 1991;144:1.
[19] Dunand DC. Mater Manuf Process 1995;10:373.
[20] Miura S, Ohashi T, Mishima Y. Intermetallics 1997;5:45.
[21] Philpot KA, Munir ZA, Holt JB. J Mater Sci 1987;22:159.
[22] Biggs DM, Bhattacharya SK. In: Metal-filled polymers. New York (NY): Marcel Dekker; 1986. p. 165.
[23] Kachelmyer CR, Varma A, Khomenko IO, Rogachev AS, Merzhanov AG. Mater Res Soc Symp Proc 1996:593.
[24] Naiborodenko YuS, Itin VI. Combust Explos Shock Wave 1975;2:343.
[25] Naiborodenko YuS, Itin VI. Combust Explos Shock Wave 1975;2:734.
[26] Maslov VM, Borovinskaya IP, Merzhanov AG. Combust Explos Shock Wave 1976;12:631.
[27] Podergin VC, Neronov VA, Iarovoi VD, Malanov MD. In: Chemical technology and metallurgy. Chernogolovka; 1975.
[28] Yeh CL, Yeh CC. J Alloys Compd 2005;388:241.
[29] Park JS, Kumsok T. Chaeryo Hakhoechi 2003;41:878.
[30] Maslov VM, Borovinskaya IP, Ziatdinov MKh. Combust Explos Shock Wave 1979;15:41.
[31] Gennari S, Maglia F, Anselmi-Tamburini U, Spinolo G. Monatsh Chem 2005;36:1871.
[32] Cunningham ME, Peddicord KL. Int J Heat Mass Transfer 1980;24:1081.
[33] Carrillo-Heian EM, Graeve OA, Feng A, Faghih JA, Munir ZA. J Mater Res 1999;14:1949.
[34] Munir ZA, Anselmi-Tamburini U. Mater Sci Rep 1989;3:277.
[35] Du Y, Chang YA, Gong W, Huang B, Xu H, Jin Z, et al. Intermetallics 2003;11:995.
[36] Servant C, Ansara I. Ber Bunsen-Gesellschaft 1998;102:1189.
[37] Dupin N, Ansara I. Rev Metall/Cah Inform Tech 1998;95:1121.
[38] Shao G. Intermetallics 2004;12:655.
[39] Weast RC, editor. Handbook of chemistry and physics. Boca Raton (FL): Chemical Rubber Co.; 1986–1987.
[40] Koh JCY, Fortini A. Int J Heat Mass Transfer 1973;16:2013.